New Journal of Physics
The open-access journal for physics

Interaction of injected dust particles with metastable neon atoms in a radio frequency plasma

H T Do[1], H Kersten[2] and R Hippler[1,3]

[1] Institut für Physik, Ernst-Moritz-Arndt-Universität Greifswald, Felix-Hausdorff-Strasse 6, 17489 Greifswald, Germany
[2] Institut für Experimentelle und Angewandte Physik, Universität Kiel, Leibnizstr 19, 24098 Kiel, Germany
E-mail: hippler@physik.uni-greifswald.de

New Journal of Physics **10** (2008) 053010 (14pp)
Received 1 February 2008
Published 7 May 2008
Online at http://www.njp.org/
doi:10.1088/1367-2630/10/5/053010

Abstract. Spatial density and temperature profiles of neon metastables produced in a radio frequency (rf) discharge were investigated by means of tunable diode laser absorption spectroscopy. The experiments were performed in the PULVA1 reactor, which is designed for the study of complex (dusty) plasmas. The line averaged measured density is about 1.5×10^{15} m^{-3} in the bulk and drops almost linearly in the plasma sheath. The gas temperature is in the range of 370–390 K. The flow of metastable atoms in the plasma sheath deduced from the spatial density distribution is dominated by the flow towards the rf electrode. The sheath length is supposed as the effective diffusion length in the plasma sheath region. This approximation was used to investigate the interaction of injected particles with the plasma. The observations and estimation provide evidence for a significant interaction between metastable atoms and powder particles which is important for energy transfer from the plasma to the particles. The power per unit area absorbed by dust particles due to the collision of metastable atoms with the dust particle surface is in the range of a few tens of mW m^{-2}.

[3] Author to whom any correspondence should be addressed.

Contents

1. Introduction

The interest in plasma–particle interactions in dusty plasmas has grown enormously during the last decade. At present, the interest is mainly caused by applied research related to materials science [1]–[3] and, recently, also with regard to plasma diagnostics [4]–[6]. Powder formation has been a critical concern for the microelectronics industry, because dust contamination can severely reduce the yield and performance of fabricated devices. Sub-micron particles deposited on the surface of process wafers can obscure device regions, cause voids and dislocations, and reduce the adhesion of thin films [7, 8].

Nowadays, dust particles are not considered as unwanted pollutants any more. Positive aspects of dusty plasmas have emerged, and they have even turned into production goods. Powders produced by plasma technology have interesting and potentially useful properties, e.g. very small sizes (nanometre to micrometre range), uniform size distribution and chemical activity. Size, structure and composition can be tailored to the specific requirements dependent on the desired application [3, 6, 9]. There are several links between dusty plasma physics and materials science. The trend is similar to the well-established plasma surface modification technology, except that now the surface of dust particles is the subject of the treatment. In these types of processing, particles are either grown in the plasma or are externally injected for subsequent treatment [10]. In particular, the increased knowledge and ability to control particles in a plasma environment has recently led to new lines of technological research, namely, the tailoring of particles with desired specific surface properties. Energetic metastables are species involved in the particle surface modification process. So far, the role and effects of metastables in dusty plasmas have not been considered to a large extent. A few years ago, Graves and co-workers measured the dust particle surface temperature and proposed a model to explain the result but the heating channel by the metastable was not taken into account [11]. There exists a lack of consideration of these species in such a plasma environment.

Tunable diode laser absorption spectroscopy (TDLAS) can support the optimization of industrial plasma processes by permitting highly specific, accurate and non-intrusive real-time monitoring of species densities. TDLAS offers significant advantages compared to conventional spectroscopy. The spectral width of the laser radiation (a few megahertz) is much smaller than the width (a few gigahertz) of the Doppler-broadened absorption profile. Sensitivity and signal-to-noise ratio are also increased in TDLAS due to the use of a high-power coherent source. The high sensitivity provides TDLAS with the ability to detect and measure gas temperature and low concentrations as successfully applied in determining the density of ground states. For

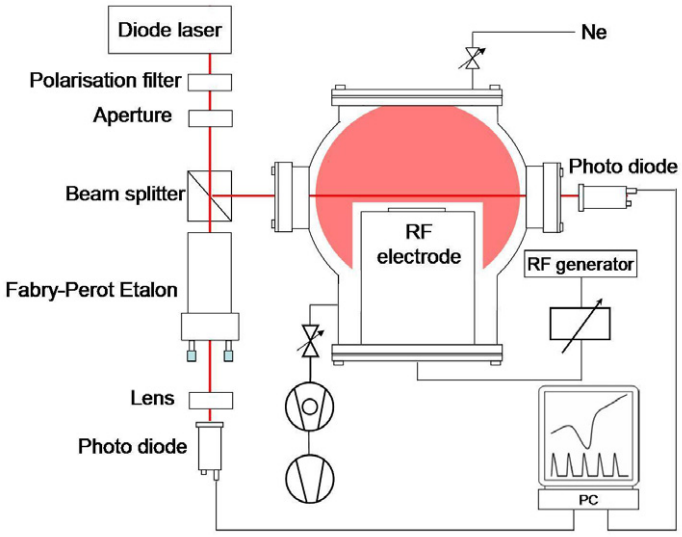

Figure 1. Experimental set-up of PULVA1 (schematic).

example, such measurements have been successfully shown during Al sputtering from a magnetron discharge [12, 13]. Moreover, an advantage of this method in studying dusty plasmas is that the presence of dust particles does not influence the metastable density measurement. The scattering and absorption effects can be taken out from the intensity profile.

In this work, the interaction between dust particles and metastable atoms is the focus of interest. The density and temperature of neon metastable atoms ($1s_3$ Ne) are measured by means of TDLAS in both pristine and dusty plasmas with injected SiO_2 micro-particles.

2. Experimental set-up

The experiments were performed in the PULVA1 reactor (figure 1) [14]–[16]. It consists of a vacuum chamber with 40 cm diameter. The chamber is pumped by a turbo molecular pump with a pumping speed of 260 litres s^{-1} that is backed by a membrane pump. The residual gas pressure is 10^{-4} Pa. Working gases are introduced into the vacuum chamber by two separate flow controllers. Neon was used as buffer gas. The discharge is driven at 13.56 MHz by a radio-frequency (rf) generator coupled to the bottom electrode by a matching network. The bottom electrode of the asymmetric rf discharge has a diameter of 13 cm and is situated near the centre of the chamber; the chamber's wall serves as the other electrode. An adjustable butterfly valve is mounted between the pump and the chamber for controlling working pressure. Measurements were carried out at working pressures of 1–10 Pa and at rf powers of 1–60 W. A copper ring with a radius of 4 or 6 cm was placed on the powered electrode to confine injected dust particles [17].

The laser system consists of a tunable single-mode diode laser and a control unit for diode temperature and diode current (Toptica DL 100). The diode laser utilizes an extended cavity laser set-up with optical feedback into the laser diode from the first order of a spectrally selective grating. The laser light passes through a polarization filter and is directed onto a beam splitter. The transmitted light is registered by a photo diode behind a Fabry–Perot etalon to monitor the light frequency [12]. The second light beam passes through the plasma chamber and is detected

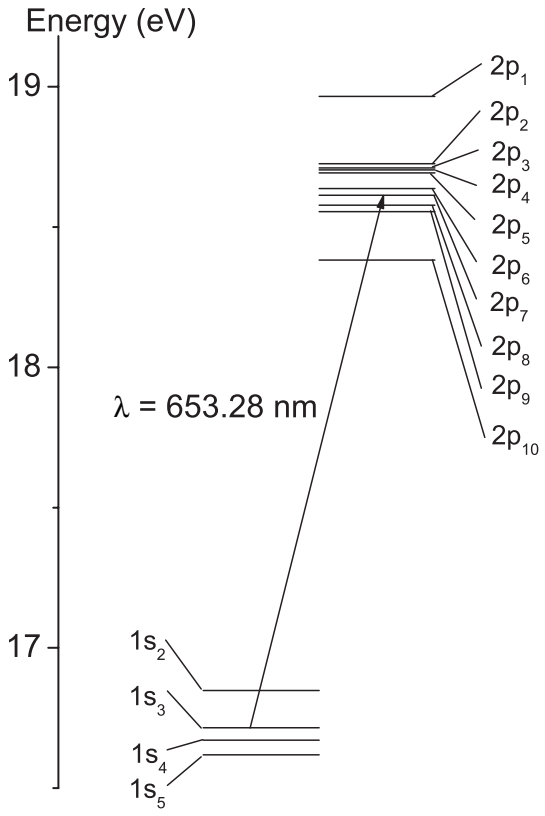

Figure 2. Neon term diagram of the 1s and 2p levels (in Paschen's notation). Values were taken from the NIST database.

by a second photodiode. The laser was tuned to the wavelength of the transition from level $1s_3$ to level $2p_7$ of neon atoms (figure 2).

Without plasma, the laser intensity, as measured by the second photodiode, linearly increases (see dashed line in figure 3). In the case of discharge operation, the photodiode signal shows pronounced variations in the neighbourhood of wavelength 653.28 nm due to absorption by excited neon atoms. The transmitted intensity follows the Lambert–Beer law of absorption [18]

$$I(\nu) = I_0(\nu) \exp\left(-\int_l \kappa(\nu, z)\,\mathrm{d}z\right), \tag{1}$$

where I_0 and I are the incident and transmitted intensity, ν is the laser frequency, κ is the absorption coefficient and l is the absorption length. The plasma occupies the whole chamber. We thus use the chamber diameter (40 cm) as the absorption length. Under the assumption of a constant Ne density inside the plasma region, equation (1) is simplified to

$$I(\nu) = I_0(\nu) \exp(-\kappa(\nu) l). \tag{2}$$

The atom density n_a is calculated from the integrated absorption profile $\kappa(\nu)$ [19]

$$n_\mathrm{a} = \frac{4\pi\varepsilon_0 m_\mathrm{e} c}{e_0^2 f \lambda_0} \sqrt{\frac{2kT}{\pi m_\mathrm{a}}} \kappa_0, \tag{3}$$

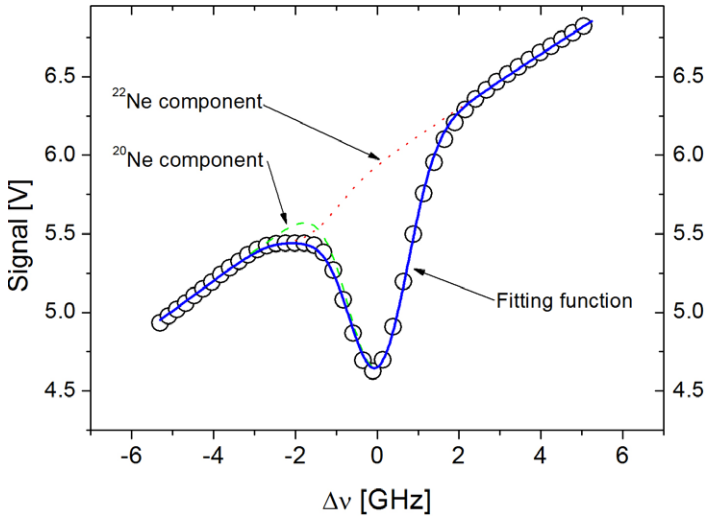

Figure 3. Sample of absorption profile and fit function (blue solid line). The contribution from the ^{20}Ne (green dashed line) and the ^{22}Ne (red dotted line) components are also shown.

where κ_0 is the absorption coefficient in the centre of the profile, ε_0 the dielectric constant, c the speed of light, m_e and e_0 electron mass and charge, respectively, m_a the atomic mass, k the Boltzmann constant, $\lambda_0 = 653.28\,\text{nm}$ the central wavelength of the investigated transition and f the optical oscillator strength for the investigated transition.

The width of the absorption signal due to Doppler broadening is related to the temperature T of Ne atoms by equation:

$$T = \frac{\lambda_0^2 m_a}{8k \ln 2} \Delta\nu^2, \tag{4}$$

where $\Delta\nu$ is the effective full-width at half maximum of the measured absorption profile. In order to account for isotope effects, the transmitted photodiode signal was fitted with a sum of two Doppler line profiles for the ^{20}Ne and ^{22}Ne components,

$$I(\nu) = (a + b\nu + c\nu^2) \exp\left\{-\kappa_0 l \exp\left[-\left(\frac{\nu - \nu_0}{0.6\Delta\nu}\right)^2\right] - \frac{\kappa_0 l}{9.326} \exp\left[-\left(\frac{\nu - \nu_0 - \nu_{iso}}{0.572\Delta\nu}\right)^2\right]\right\}. \tag{5}$$

The parameters a, b and c represent the baseline of the signal, i.e. the transmitted signal without plasma, approximated by a second-order polynomial. ν_0 is the central frequency, taken as a free fit parameter, $\Delta\nu_{iso}$ is the isotope shift of the ^{22}Ne component. A typical least-squares fit result is displayed in figure 3 together with the measured signal. The fit quality is excellent with deviations on a point-to-point comparison of less than 1%. The overall accuracy of the extracted temperature derived from equation (4) is typically 2–5 K. The accuracy of the obtained atom density derived via equation (3) is essentially determined by the estimated accuracy of the underlying oscillator strength f of ±25%, an estimated accuracy of the absorption length inside the plasma of ±5% and a negligible statistical uncertainty of less than 0.1%, adding up to an estimated overall accuracy for the absolute mean neon atom density of about ±30%.

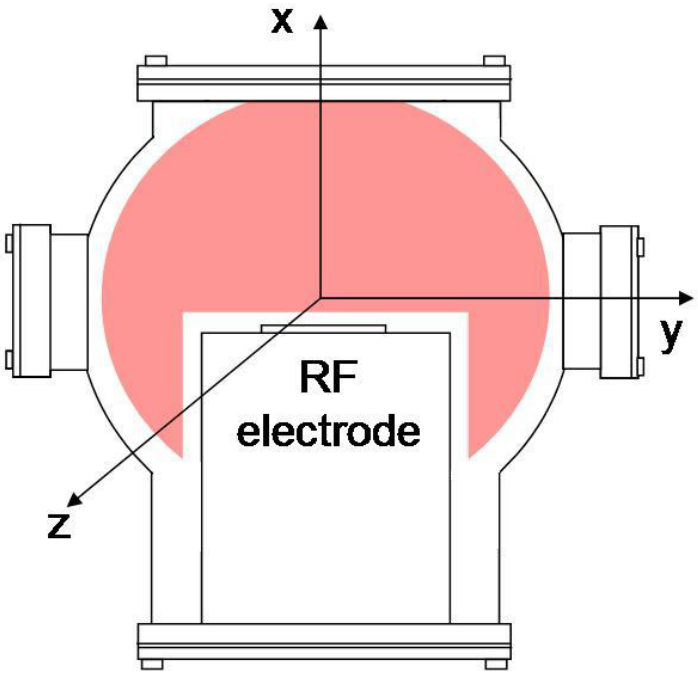

Figure 4. The coordinate system in the plasma chamber.

The rf discharge was spatially analysed at different plasma conditions. Three types of experiments were carried out. First, the laser beam was shining along the y-direction (figure 4) and scanned horizontally (along the z-direction) at two heights above the rf electrode: 1 cm (position of the plasma sheath); 2 cm (inside the plasma bulk). During the measurement, all external conditions such as plasma power, pressure and gas flow were kept constant. From this measurement, the radial distribution of neon metastable atom density $n_m(x, z)$ and temperature is obtained. Similarly, in order to monitor the axial neon metastable atom distribution $n_m(x, 0)$, the laser beam was fixed at $z = 0$ and moved along the x-direction.

In the second type of measurements, the effect of gas pressure on metastable density and temperature was examined. The laser beam was fixed in one position ($z = 0$, $y = 0$, and at different heights x) while the plasma conditions were varied.

And finally, in order to study the influence of particles on the plasma, relatively large SiO_2 particles (10 μm) were injected into the plasma. They were confined in the sheath boundary, about 1.5 cm above the rf electrode. The laser beam was placed at this height and moved radially to monitor the radial metastable density in the presence of dust particles. In addition, the laser beam was placed in the centre and moved along the x-direction to measure the axial density.

3. Results and discussions

3.1. Plasma characterization

The Ne metastable atom density in PULVA1 was observed to be radially and axially inhomogeneous. Typical values are a few 10^{15} m^{-3} in the bulk and some 10^{14} m^{-3} in the plasma sheath. The radial distribution can be fitted by a Gaussian profile giving a full width at half maximum $w \sim 14$ cm (figure 5). The axial density increases almost linearly from electrode

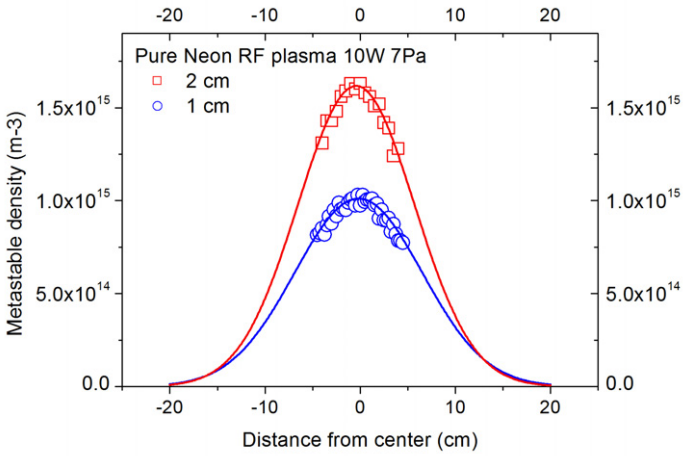

Figure 5. Measured radial distribution of the neon metastable density and corresponding Gaussian fits for two distances above the electrode.

to plasma bulk. The density gradually decreases towards the wall chamber, and reaches a maximum in the bulk plasma. By comparing the axial distributions of neon metastable density at different pressures, we can clearly observe the expansion of the plasma sheath with decreasing plasma pressure (figure 6) [20]. The gas temperature is, however, nearly constant in the whole plasma with a value of about 380 K. There is only a small increase of about 10 K near the rf electrode.

Assuming that the metastable density distribution follows a Gaussian profile and accounting for the fact that the plasma is radially symmetric, the metastable density $n_m(x, y, z)$ at normalized coordinates x, y and z can be written as

$$n_m(x, y, z) = n_m(x, 0, 0) \exp\left(-\frac{y^2 + z^2}{2\sigma^2}\right), \tag{6}$$

where σ is related to the full width at half maximum w of the Gaussian distribution by

$$w = 2\sqrt{2 \ln 2}\,\sigma. \tag{7}$$

The measured density at height x above the electrode and distance z from the plasma centre $n_m(x, z)$, therefore, is equal to:

$$n_m(x, z) = n_m(x, 0) \exp\left(-\frac{z^2}{2\sigma^2}\right), \tag{8}$$

where $n_m(x, 0)$ is the measured metastable density in the centre at height x. Since $\sigma < R_r$, we get

$$\int_{-R_r}^{+R_r} \exp\left(-\frac{y^2}{2\sigma^2}\right) dy \approx \int_{-\infty}^{+\infty} \exp\left(-\frac{y^2}{2\sigma^2}\right) dy = \sigma\sqrt{2\pi}, \tag{9}$$

where R_r is the chamber radius.

Combining the radial distribution of the metastable density (equation (8)) with the measured axial distribution $n_m(x)$, the spatial density distribution of the metastable atoms can

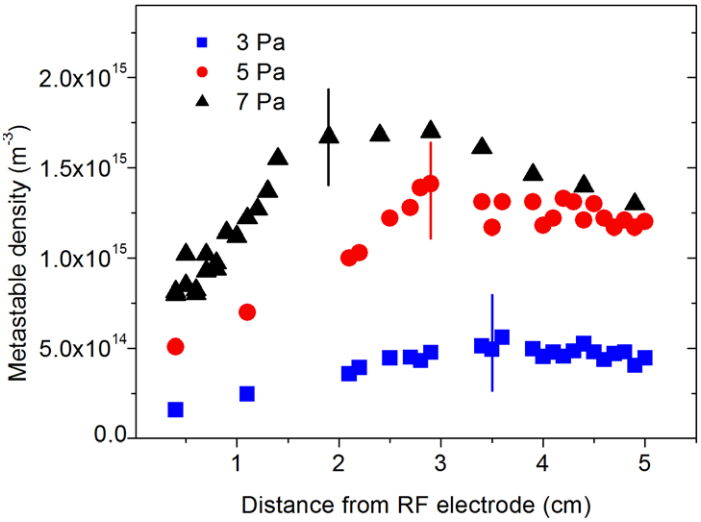

Figure 6. Axial distribution of neon metastable density at different pressures. Vertical lines indicate the sheath boundaries.

be written as:

$$n_{\mathrm{m}}(x, y, z) = \frac{2R_{\mathrm{r}}n_{\mathrm{m}}(x)}{\sigma\sqrt{2\pi}} \exp\left(-\frac{y^2+z^2}{2\sigma^2}\right). \tag{10}$$

The diffusive flow of metastable atoms in the plasma sheath deduced from the spatial distribution of metastable density is dominated by the flow towards the electrode, since the sheath length (about 1.5 cm) is much smaller than the width of the Gaussian distribution in y- and z-directions (about 14 cm).

Neon metastable density and temperature were also characterized in relation to the plasma power and gas pressure. The metastable atom density increases significantly with plasma power. This increase is more pronounced in the plasma centre compared to the plasma sheath. At 7 Pa, it readily reaches a plateau of about $2.8 \times 10^{15}\,\mathrm{m}^{-3}$ (at 40 W power-input in the plasma bulk), while it is still increasing in the sheath region. The temperature does not change significantly with plasma power, e.g. it increases from 370 to 390 K in the plasma glow, whereas it remains approximately constant in the plasma sheath (figure 7). In the examined pressure range (2–10 Pa), the density of electrons which are responsible for the formation of metastable atoms increases with increasing pressure [21] and the metastable atom density, hence, also increases with pressure (figure 8). The metastable atom temperature remains largely unaffected by a pressure increase.

3.2. Interaction of metastable atoms with dust particles

In this section, we present results for a dusty plasma where the dust particles (silicon oxide of 10 μm diameter) are injected from outside into the plasma. By the combined action of electrostatic and gravitational forces, the grains are trapped in the plasma sheath adjacent to the glow [22]. Two copper rings with different radii (4 or 6 cm) are used to confine the particles. The radii of the confined dust clouds R_{c} are about 3 and 5 cm for the small and the large rings, respectively. With the larger confining ring, it is possible to capture a larger dust cloud with a

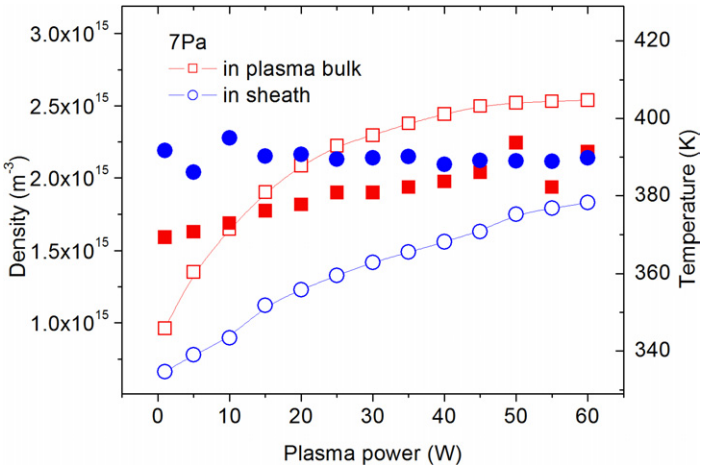

Figure 7. Dependences of neon metastable density and temperature on plasma power. The filled circles and squares represent the temperature, the open circles and squares represent the density.

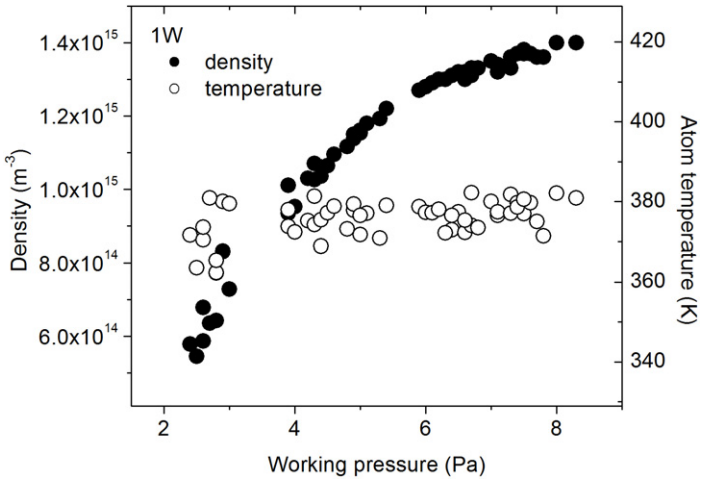

Figure 8. Dependences of neon metastable density and temperature on gas pressure.

higher dust density. Therefore, the effect of dust particles on the metastable atom density can be enhanced and becomes easier to observe.

The spatial distribution of metastable atoms in a dust-containing plasma was measured and compared to that of pristine plasmas under the same plasma conditions. It is believed that the metastable density in the dusty plasma is higher when compared to pristine plasma [23]. However, when the dust density is low and the dust surface is large which is the case in the present work, the loss effect overcompensates the enhancement resulting in a lower metastable density in the dusty plasma. The line integrated metastable atom density within the dust cloud drops significantly ($0.5 \times 10^{14}\,\mathrm{m}^{-3}$ for the small ring and $3.5 \times 10^{14}\,\mathrm{m}^{-3}$ for the large ring) in comparison to that of dust-free plasma at the same conditions and positions (figures 9 and 10).

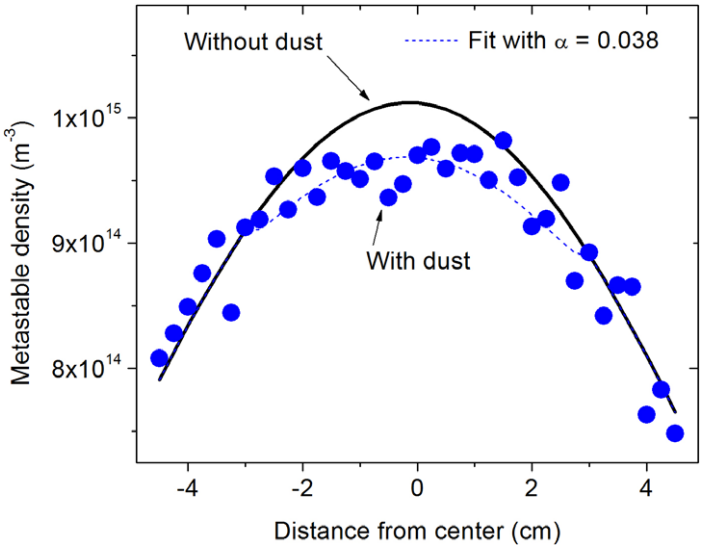

Figure 9. Radial neon metastable density of dusty plasma compared to those of the pristine plasma at the same conditions and locations with a small ring.

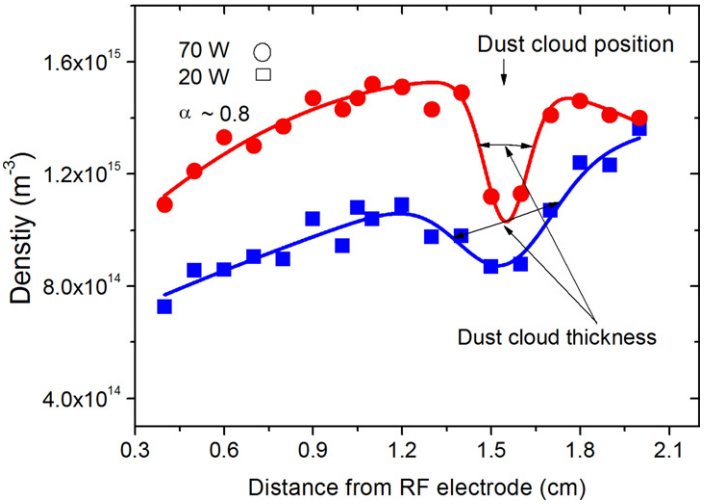

Figure 10. Axial neon metastable density of dusty plasma with a 6 cm ring.

The decreasing metastable atom (Ne^*) density provides evidence for a significant interaction between metastable atoms and particles. The micro-particles act as quenching agents in the energy transfer process:

$$Ne^* + \text{particle} \rightarrow Ne + \text{particle(heated)}. \quad (11)$$

Metastable atoms which carry an internal energy of about 16.715 eV should thus play a considerable role in the heating of dust particles confined by a plasma.

Considering a simple corona model, metastable atoms are generated by direct excitation of ground state neon atoms by impact of energetic electrons and lost by diffusion to the electrodes and to the dust particles. The de-excitation of metastables in collision with cold electrons is neglected since the electron density in the plasma sheath is small. The density of metastable

atoms within the dust cloud is therefore given by the relation:

$$\frac{\partial n_{\mathrm{m}}(x,y,z)}{\partial t} = k_{\mathrm{m}} n_0 n_{\mathrm{e}} - \frac{2D_{\mathrm{m}}}{l_{\mathrm{eff}}^2} n_{\mathrm{m}}(x,y,z) - \frac{2D_{\mathrm{m}}}{l_{\mathrm{D}}^2} n_{\mathrm{m}}(x,y,z). \tag{12}$$

Here, n_0 and n_{m} are ground state and metastable state density, respectively, of neon atoms, n_{e} is the electron density, and k_{m} is the rate coefficient for electron impact excitation from the ground state to the metastable state. The second and third terms in the right-hand side of equation (12) are the losses by diffusion to the chamber wall and to dust particles, respectively, with corresponding effective lengths l_{eff} and l_{D}, and D_{m} is the diffusion coefficient of metastable neon atoms in neon. The ground state atom density is approximately equal to the neutral gas density of neon and thus independent of the presence of particles.

For a dust-free plasma, the loss of metastable atoms by diffusion in the plasma sheath is dominated by the flow towards the electrode. Hence, the sheath length l_{sh} can reasonably be used as the effective length.

For a dust particle-containing plasma an additional loss of metastable atoms at the surface of grains occurs; the effective length is

$$l_{\mathrm{D}} = \frac{V}{S} = \frac{N_{\mathrm{D}}/n_{\mathrm{D}}}{N_{\mathrm{D}} S_{\mathrm{D}}} = \frac{1}{n_{\mathrm{D}} S_{\mathrm{D}}}, \tag{13}$$

where V is the dust cloud volume, S is the total dust surface area, N_{D} is the total number of dust particles in the dust cloud, n_{D} is the dust density and S_{D} is the surface area of one particle, respectively.

With this approach, we obtain the following relation between the steady state density in the plasma sheath for the cases with ($n_{\mathrm{m}}^{\mathrm{D}}$) and without dust particles (n_{m}):

$$n_{\mathrm{m}}^{\mathrm{D}}(x,y,z) = \frac{1}{1+\alpha} n_{\mathrm{m}}(x,y,z), \tag{14}$$

with

$$\alpha^{1/2} = l_{\mathrm{eff}}/l_{\mathrm{D}} = l_{\mathrm{sh}} n_{\mathrm{D}} S_{\mathrm{D}}. \tag{15}$$

The so-called quenching factor α accounts for the loss of metastable atoms due to the presence of dust particles; it becomes zero for a dust-free plasma, e.g. outside the dust particle cloud.

The quenching factor is estimated from the measured radial distributions in dust-free ($n_{\mathrm{m}}(x,z)$) and dust-containing ($n_{\mathrm{m}}^{\mathrm{D}}(x,z)$) plasmas, together with the radius of the dust cloud R_{c}. The measured metastable density in the presence of dust particles can be written as:

$$\begin{aligned} n_{\mathrm{m}}^{\mathrm{D}}(x,z) &= \int_{-R_{\mathrm{r}}}^{+R_{\mathrm{r}}} n_{\mathrm{m}}(x,y,z)\,\mathrm{d}y - \int_{-\sqrt{R_{\mathrm{c}}^2-z^2}}^{+\sqrt{R_{\mathrm{c}}^2-z^2}} \{n_{\mathrm{m}}(x,y,z) - n_{\mathrm{m}}^{\mathrm{D}}(x,y,z)\}\,\mathrm{d}y \\ &= n_{\mathrm{m}}(x,z) - \frac{\alpha}{1+\alpha} n_{\mathrm{m}}(x,0) \exp\left(-\frac{z^2}{2\sigma^2}\right) \int_{-\sqrt{R_{\mathrm{c}}^2-z^2}}^{+\sqrt{R_{\mathrm{c}}^2-z^2}} \exp\left(-\frac{y^2}{2\sigma^2}\right) \mathrm{d}y \\ &= n_{\mathrm{m}}(x,z) - \frac{\alpha}{1+\alpha} K(z) n_{\mathrm{m}}(x,0). \end{aligned} \tag{16}$$

The quenching factor is expressed as follows:

$$\alpha = \frac{\Delta n_m(x,z)}{K(z) n_{\mathrm{m}}(x,0) - \Delta n_{\mathrm{m}}(x,z)}, \tag{17}$$

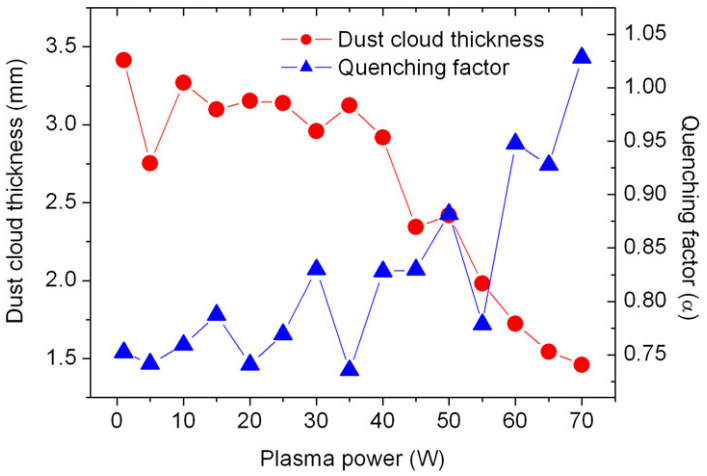

Figure 11. Quenching factor and corresponding dust cloud thickness with a confining ring of 6 cm radius at different plasma power.

where $\Delta n_{\mathrm{m}}(x, z) = n_{\mathrm{m}}(x, z) - n_{\mathrm{m}}^{\mathrm{D}}(x, z)$ is the difference of measured metastable densities between the dusty plasma and the dust-free plasma.

Since R_{c} is smaller than σ, we can use the following approximation for $K(z)$:

$$K(z) \approx \frac{1}{\sigma}\sqrt{\frac{2}{\pi}}\sqrt{R_{\mathrm{c}}^2 - z^2}\left[\exp\left(-\frac{R_{\mathrm{c}}^2 - z^2}{2\sigma^2}\right) + 1\right]. \tag{18}$$

At different positions within the dust cloud the calculated results give almost the same value of $\alpha = 0.038$ for a neon dusty plasma of 10 W rf power, 7 Pa gas pressure and with a 4 cm radius confining ring (figure 9). In our experiments, l_{sh} is estimated from the axial distribution of metastable density of about 1.5 cm and S_{D} equals $3.14 \times 10^{-10}\,\mathrm{m}^{-2}$ for 10 μm dust particles. The dust density n_{D} is, therefore, about $4.14 \times 10^{10}\,\mathrm{m}^{-3}$ which corresponds to 42 particles per cubic millimetre.

However, with increasing plasma power, the dust cloud thickness decreases due to the increased wakefield attraction force [24], which compresses the dust cloud in the x-direction. The increase of the quenching factor is in agreement with the decreasing dust cloud thickness, which is associated with an increasing dust particle density (figure 11). The dust cloud thickness is deduced from the axial distribution of metastable density in the presence of dust particles (figure 10). The estimated dust density using equation (15) with the calculated α increases from 200 to 440 particles per cubic millimetre.

In order to calculate the particle heating by metastable atoms, the metastable density $n_{\mathrm{m}}^{\mathrm{D}}$ around the dust particles should be known. This quantity is calculated from equation (14) using the radial distribution of pristine plasma together with the quenching factor. Assuming the energy transfer probability of metastables to be unity, the power per unit area absorbed by dust particles due to the collision of metastable atoms with dust particle surfaces P_{m} [5, 25] can be written as:

$$P_{\mathrm{m}} = 0.25\varepsilon n_{\mathrm{m}}^{\mathrm{D}}(x, y, z)\sqrt{\frac{8k_{\mathrm{B}}T}{\pi m_{\mathrm{a}}}} = 8.07 \times 10^{-19}\frac{1}{1+\alpha}n_{\mathrm{m}}(x, y, z)\sqrt{T}, \tag{19}$$

where ε is the energy of the metastable level (16.715 eV for level $1s_3$ of neon). At 10 W plasma power, within the dust cloud n_m is of the order of $2.66 \times 10^{15}\,m^{-3}$ and T is of the order of 380 K, thus the energy influx is $0.04\,W\,m^{-2}$ in the case of the small cloud and about 0.03 ($W\,m^{-2}$) in the case of the large ring where we have a lower metastable density (large cloud). The energy transfer by the metastables is in the same order as the contributions of kinetic energy of ions and electrons and the energy released by their recombination on the grain surface [5].

4. Conclusion

The radial distribution of metastable atom density in a capacitively coupled rf discharge can be approximated to a Gaussian profile with width much smaller than the plasma chamber diameter. The diffusion flow of metastable atoms deduced from their spatial density distribution gives the loss of metastable atoms in the plasma sheath mostly contributed by flow towards the electrode. This approximation was used to investigate the experimental results for a dusty plasma with injected SiO_2 particles trapped in the plasma sheath. The quenching factor α which accounts for the interaction between dust particles and metastable atoms was estimated to be of the order of 0.038 for the case of a small ring (4 cm radius) and the corresponding estimated dust density $1.3 \times 10^9\,m^{-3}$. Meanwhile with a bigger ring which confined higher dust density, the factor becomes large (about 0.8).

The particle heating by metastable atoms was strongly evidenced. The quenching factor was then used to calculate the power per unit area absorbed by dust particles due to bombardment of metastable atoms onto dust particle surfaces P_m. In our experiments, P_m is about $0.04\,W\,m^{-2}$ for the low dust density case and smaller for higher dust density.

Acknowledgments

Part of this work was supported by the Deutsche Forschungsgemeinschaft through SFB/TR 24.

References

[1] Selwyn G S, McKillop J S, Haller K L and Wu J J 1990 *J. Vac. Sci. Technol.* A **8** 1726
[2] Bouchoule A ed 1999 *Dusty Plasmas: Physics, Chemistry and Technological Impacts in Plasma Processing* (New York: Wiley)
[3] Stoffels E, Stoffels W W, Kersten H, Swinkels G H P M and Kroesen G M W 2001 *Phys. Scr.* T **89** 168
[4] Law D A, Tomme E B, Steel W H, Anaratonne B M and Allen J E 1999 *Proc. XXIV ICPIG, Proc. IV/109* (*Warsaw, Poland*)
[5] Swinkels G H P M, Kersten H, Deutsch H and Kroesen G M W 2000 *J. Appl. Phys.* **88** 1747
[6] Kersten H, Deutsch H, Stoffels E, Stoffels W W and Kroesen G M W 2003 *Int. J. Mass Spectrom.* **223–224** 313
[7] Selwyn G S, Singh J and Benett R S 1988 *J. Vac. Sci. Technol.* A **7** 2758
[8] Bouchoule A 1993 *Phys. World* **6** 47
[9] Kersten H, Schmetz P and Kroesen G M W 1998 *Surf. Coat. Technol.* **108/109** 507
[10] Kersten H, Deutsch H, Stoffels E, Stoffels W W, Kroesen G M W and Hippler R 2001 *Contrib. Plasma Phys.* **41** 598
[11] Daugherty J E and Graves D B 1993 *J. Vac. Sci. Technol.* A **11** 1126
[12] Wolter M, Tung Do H, Steffen H and Hippler R 2005 *J. Phys. D: Appl. Phys.* **38** 2390–5
[13] Olejnicek J, Do H T, Hubicka Z and Jastrabik R H L 2006 *Japan J. Appl. Phys.* **45**

[14] Kersten H, Thieme G, Fröhlich M, Bojic D, Tung D H, Quaas M, Wulff H and Hippler R 2005 *Pure Appl. Chem.* **77** 415–28
[15] Kersten H *et al* 2003 *New J. Phys.* **5** 93
[16] Matyash K, Fröhlich M, Kersten H, Thieme G, Schneider R, Hannemann M and Hippler R 2004 *J. Phys. D: Appl. Phys.* **37** 2703
[17] Thieme G, Basner R, Wiese R and Kersten H 2008 *Faraday Discuss.* **137** 157
[18] Demtröder W 2000 *Laserspektroskopie* (Berlin: Springer)
[19] Scheibner H, Franke S, Solyman S, Behnke J F, Wilke C and Dinklage A 2002 *Rev. Sci. Instrum.* **73** 378
[20] Kersten H, Stoffels E, Stoffels W W, Otte M, Csambal C, Deutsch H and Hippler R 2000 *J. Appl. Phys.* **87** 3637
[21] Tatanova M, Thieme G, Basner R, Hannemann M, Golubovskii Yu B and Kersten H 2006 *Plasma Sources Sci. Technol.* **15** 507
[22] Vladimirov S V, Ostrikov K and Samarian A A 2005 *Physics and Applications of Complex Plasmas* (London: Imperial College Press)
[23] Denysenko I, Berndt J, Kovacevic E, Stefanovic I, Selenin V and Winter 2006 *J. Phys. Plasmas* **13** 073507
[24] Melzer A, Schweigert A V and Piel A 2000 *Phys. Scr.* **61** 495
[25] Piejak R, Godyak V, Alexandrovich B and Tishchenko N 1998 *Plasma Sources Sci. Technol.* **7** 590